

Cite this: *Chem. Sci.*, 2023, 14, 3352

All publication charges for this article have been paid for by the Royal Society of Chemistry

Received 16th September 2022  
Accepted 27th February 2023

DOI: 10.1039/d2sc05200h

rsc.li/chemical-science

# Cobalt-catalyzed radical-mediated carbon–carbon scission *via* a radical-type migratory insertion†

Jian-Biao Liu,<sup>\*a</sup> Xiao-Jun Liu,<sup>id a</sup> João C. A. Oliveira,<sup>b</sup> De-Zhan Chen<sup>id a</sup> and Lutz Ackermann<sup>id \*b</sup>

Migratory insertions of alkenes into metal–carbon (M–C) bonds are elementary steps in diverse catalytic processes. In the present work, a radical-type migratory insertion that involves concerted but asynchronous M–C homolysis and radical attack was revealed by computations. Inspired by the radical nature of the proposed migratory insertion, a distinct cobalt-catalyzed radical-mediated carbon–carbon (C–C) cleavage mechanism was proposed for alkylidenecyclopropanes (ACPs). This unique C–C activation is key to rationalizing the experimentally observed selectivity for the coupling between benzamides and ACPs. Furthermore, the C(sp<sup>2</sup>)–H activation in the coupling reaction occurs *via* the proton-coupled electron transfer (PCET) mechanism rather than the originally proposed concerted metalation–deprotonation (CMD) pathway. The ring opening strategy may stimulate further development and discovery of novel radical transformations.

## Introduction

Migratory insertion reactions are fundamental elementary steps involved in a variety of commonly practiced catalytic reactions. Numerous investigations have been conducted to identify the detailed mechanism and the kinetic and thermodynamic behavior of these transformations to disclose the basic principles and to design more efficient catalysts.<sup>1</sup> Among the various insertions, migratory insertion of alkenes into metal–carbon (M–C) bonds is one of the most efficient methods to form new carbon–carbon (C–C) bonds (Scheme 1a). Prominent examples include the palladium-catalyzed Mizoroki–Heck coupling<sup>2</sup> as well as the catalytic insertion polymerization.<sup>3</sup> The generally accepted mechanism for alkene insertion relies on a four-center transition state. During this 2 $\pi$  + 2 $\sigma$  reaction, the occupied  $\sigma_{M-C}$  and  $\pi_{alkene}$  orbitals interact with the vacant  $\pi_{alkene}^*$  and  $\sigma_{M-C}^*$  orbitals, respectively, leading to the formation of new M–C and C–C bonds.<sup>4</sup>

Adenosylcobalamin, also known as coenzyme B12, is a naturally occurring organometallic complex that plays a pivotal role in a number of metalloenzyme-catalyzed radical

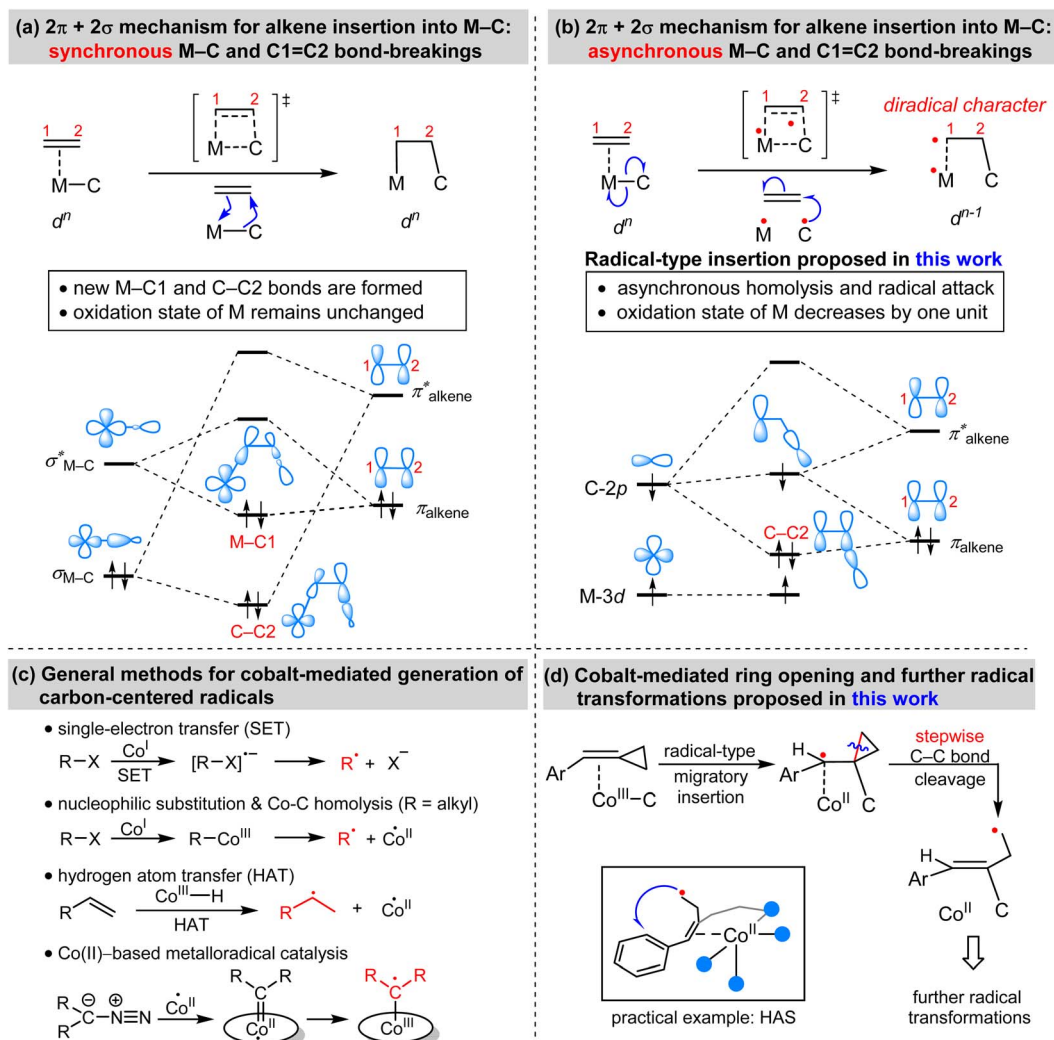
reactions.<sup>5</sup> The low bond-dissociation energy (BDE) of the axial Co–C bond in coenzyme B12 results in its facile homolytic cleavage, which plays an important role in the observed biological activities. Utilizing this kind of one-electron reactivity of cobalt and other first-row transition metals, synthetic chemists have explored different highly controlled radical reactions.<sup>6</sup> Inspired by the one-electron reactivity of first-row transition metals, we anticipated that the alkene insertion may proceed *via* a concerted but asynchronous M–C homolysis and radical attack (Scheme 1b), which is distinct from the synchronous M–C and C=C bond-breakings. This radical-type insertion involves a three-orbital interaction. Meanwhile, the insertion products exhibit a diradical character with a decrease of the physical oxidation state of the metal. To the best of our knowledge, this radical-type migratory insertion has thus far proven elusive, while it could provide an efficient access to carbon-centered radicals.

Transition-metal-mediated radical reactions have provided various innovative catalysis protocols for organic synthesis.<sup>7</sup> In this context, the contribution of cobalt in radical chemistry is remarkable because of its cost effectiveness and unique catalytic reactivity.<sup>8</sup> In general, the methods for the cobalt-mediated generation of carbon-centered radicals can be classified into the following types: single-electron transfer (SET), nucleophilic substitution and Co–C homolysis, hydrogen atom transfer (HAT), and metalloradical catalysis (Scheme 1c).<sup>9</sup> Based on detailed consideration of the mechanistic information of the aforementioned radical-type migratory insertion as well as the classical radical clock reactions, we were wondering whether alkylidenecyclopropanes (ACPs) could exhibit new reactivity patterns. As a result, we, herein, demonstrate an unprecedented

<sup>a</sup>College of Chemistry, Chemical Engineering and Materials Science, Shandong Normal University, Jinan 250014, China. E-mail: jianbiaoliu.thu@sdu.edu.cn

<sup>b</sup>Institut für Organische und Biomolekulare Chemie, Wöhler Research Institute for Sustainable Chemistry (WISCh), Georg-August-Universität Göttingen, Tammannstraße 2, 37077 Göttingen, Germany. E-mail: Lutz.Ackermann@chemie.uni-goettingen.de

† Electronic supplementary information (ESI) available: Additional computational results, calculated energies and imaginary frequencies, and Cartesian coordinates of optimized structures. See DOI: <https://doi.org/10.1039/d2sc05200h>



Scheme 1 (a) Classical mechanism for the migratory insertions of alkenes into M–C bonds. (b) Proposed radical-type insertion mechanism. (c) General methods for cobalt-mediated generation of carbon-centered radicals. (d) Proposed cobalt-mediated ring opening strategy.

strain-release generation of radicals *via* a cobalt-catalyzed radical-mediated C–C bond cleavage/functionalization strategy (Scheme 1d). The resulting homoallyl radical can enable aromatic C–H functionalization such as homolytic aromatic substitution (HAS) reactions, as illustrated by an example of cobalt-catalyzed coupling between benzamides and ACPs.<sup>10</sup> This cobalt-mediated ring opening reaction represents a fundamentally distinct strategy to generate carbon-centered radicals, with considerable potential for the development of new types of radical transformation.

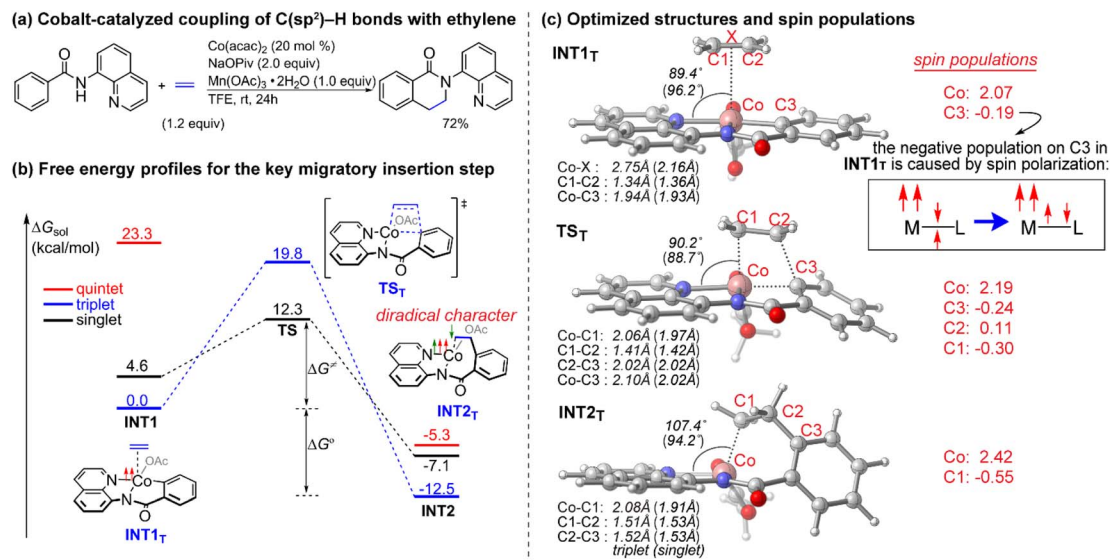
## Results and discussion

### Mechanism for migratory insertion of ethylene into Co–C bonds

Since the pioneering discovery of the 8-aminoquinoline-directed Co-catalyzed C–H alkenylation,<sup>11</sup> diverse cobalt-catalyzed C(sp<sup>2</sup>)–H annulations with alkenes, alkynes, allenes, and heterocycles were realized by different groups.<sup>12–17</sup> We

initiated our investigation by exploring the cobalt-catalyzed coupling of C(sp<sup>2</sup>)–H bonds with ethylene as the model reaction, as was reported by Daugulis<sup>12a</sup> (Fig. 1a). The calculated reaction profiles of migratory insertion of alkene are depicted in Fig. 1b. Additional computational results are given in Fig. S1–S8 in the ESI.† All three possible spin states of Co(III) were investigated, *i.e.*, the singlet ( $S = 0$ ), triplet ( $S = 1$ ), and quintet ( $S = 2$ ) states. For the alkene-coordinated complex **INT1**, the medium-spin triplet is the ground state, which lies below the low-spin singlet and high-spin quintet states by 4.6 kcal mol<sup>−1</sup> and 23.3 kcal mol<sup>−1</sup>, respectively. The migratory insertion transition state **TS**, however, exhibits a different energy ordering, with the closed-shell singlet being 7.5 kcal mol<sup>−1</sup> more stable than the triplet. Attempts to locate the corresponding quintet transition state from the  $\pi$  complex were unsuccessful. The relative energy of the resulting triplet insertion product **INT2<sub>T</sub>** is lower than the other two states, which results in larger reaction energy of the triplet state. The reaction pathway of the alkene insertion into Co–C bond has the characteristic features of a two-state





**Fig. 1** (a) Cobalt-catalyzed coupling of C(sp<sup>2</sup>)–H bonds with ethylene. (b) Free energy profiles for the migratory insertion of ethylene into Co–C bonds calculated at the SMD(TFE)/B3LYP–D3(BJ)/def2-TZVP//SMD(TFE)/B3LYP–D3(BJ)/6-31G(d,p)/SDD(Co) level of theory. (c) Optimized structures of the intermediates and transition states with selected bond lengths, angles (values for the singlets are given in parentheses) and spin populations.

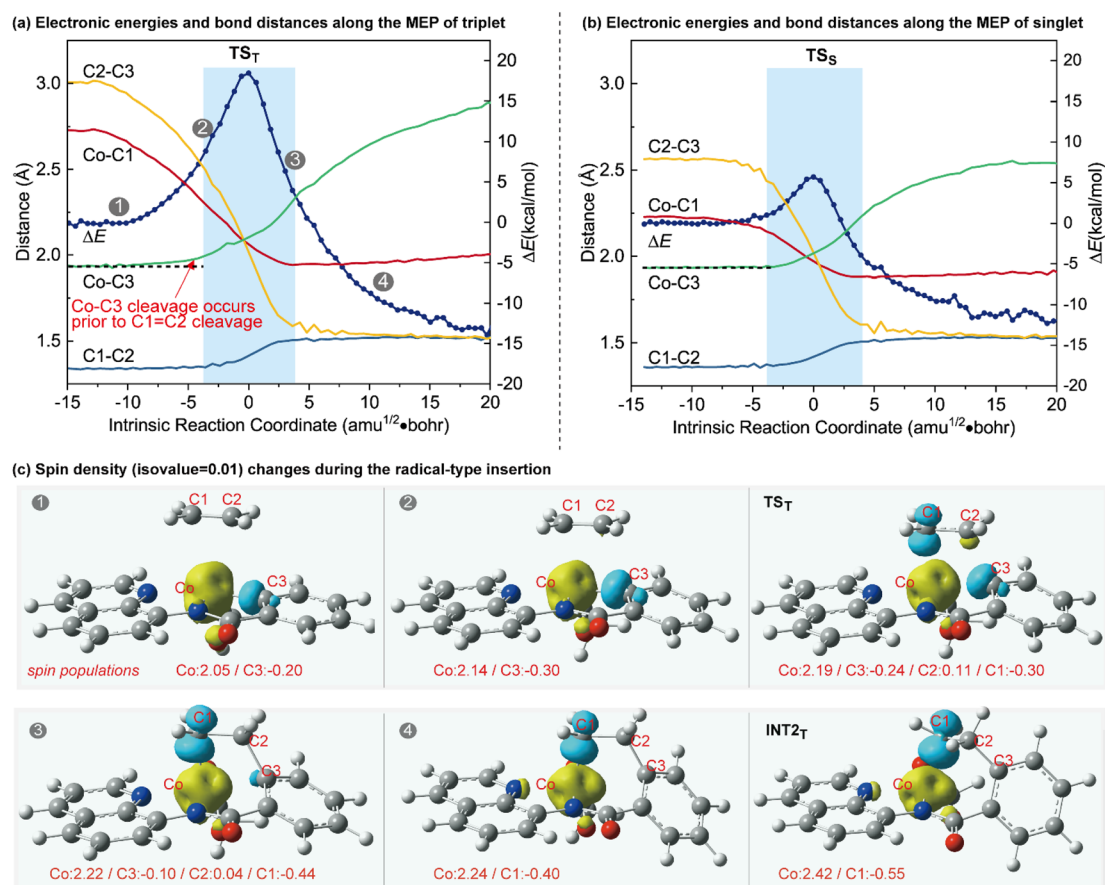


Fig. 2 Electronic energies and bond distances along the MEP of the (a) triplet state and (b) singlet state. (c) The spin density contours (isovalue = 0.01, yellow:  $\alpha$ -spin density, cyan:  $\beta$ -spin density) and spin population changes during the radical-type insertion.

reactivity (TSR) scenario,<sup>18</sup> in which the initially medium-spin triplet crosses over through the singlet transition state to generate the insertion intermediate.

The optimized structures of the intermediates and transition states are shown in Fig. 1c. The Mulliken atomic spin populations, representing the excess of positive ( $\alpha$ ) or negative ( $\beta$ ) spin on an atomic site, are also provided. For the alkene-coordinated complex **INT1**, the metal–olefin bond distance in the triplet is significantly longer than that of the singlet. The spin population for Co in **INT1<sub>T</sub>** is 2.07, very close to the number of unpaired electrons (2 electrons with  $\alpha$ -spin) for the complex. The negative spin population for C3 atom in **INT1<sub>T</sub>** is caused by spin polarization,<sup>19</sup> which makes the bonding electron pair of equatorial Co–C3 polarized. Consequently, a certain amount of the positive spin density of the bonding electron pair gets close to the metal atom, whereas some negative spin densities are induced at the atoms bonded to the metal. In the transition state **TS<sub>T</sub>**, the absolute values of spin population on Co and C3 atoms both increase as compared to that in **INT1<sub>T</sub>**. Furthermore, in **TS<sub>T</sub>** an excess on the spin density distribution of 0.11 for the  $\alpha$ -spin and 0.30 for the  $\beta$ -spin was found on C2 and C1 atoms, respectively. For the resulting insertion intermediate, it is noteworthy that the Co–C1 bond in the **INT2<sub>T</sub>** is 0.17 Å longer than that in the **INT2<sub>S</sub>** with the carbon atom presenting a slight deviation from the axial position (Fig. 2c). More interestingly, spin population analysis revealed a 0.55 excess of the  $\beta$ -spin at the C1 atom and a significant spin density of 2.42 located on the cobalt metal center.


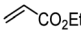
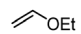
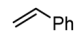
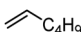
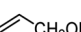

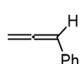
### The radical-type migratory insertion

To further illustrate the distinctions between the proposed radical-type migratory insertion and the conventional process, the key bond distances along the minimum energy path (MEP) were examined in detail (Fig. 2). The results of the triplet and singlet states correspond to the radical-type and the classical synchronous mechanisms, respectively. Herein, we focus on the breaking of C1=C2 and Co–C3 bonds to inspect the beginning of the insertion process. A comparison of the bond distance changes during the two different mechanisms reveals that they are both energetically concerted but the C1=C2 and Co–C3 bond-breakings in the radical-type migratory insertion are asynchronous<sup>20</sup> (Fig. 2a). The homolytic Co–C3 bond breaking occurs prior to the C1=C2 breaking in the radical-type mechanism (Fig. 2a), which is distinct from bond breaking events occurring synchronously in Fig. 2b. The differences between the two mechanisms are also well reflected by the changes of the aromaticity. The aromaticity decreases along the MEP for the conventional mechanism on the basis of the calculated nucleus-independent chemical shift (NICS) values at the ring center NICS(0).<sup>21</sup> However, in the radical-type mechanism, the aromaticity first gradually increases before the highest energy point following a decrease during the insertion process (Fig. S4†). The spin density changes along the MEP of the triplet state shown in Fig. 2c clearly demonstrate the electron-transfer process during the concerted but asynchronous Co–C homolysis and radical attack, which is in good agreement with the

orbital interaction analysis in Scheme 1b. The spin density contour and spin population for **INT2<sub>T</sub>** show an unpaired spin density on the Co and the C1 atoms, with opposite signs, suggesting that this intermediate presents a diradical character.<sup>22</sup> Accordingly, the stable **INT2<sub>T</sub>** complex can be better described as a quartet cobalt(II) antiferromagnetically coupled with a carbon-centered radical.

To investigate the substituent effect on the feasibility of the radical-type insertion mechanism, the computed activation free energies and free energy changes during the migratory insertion step of various monosubstituted alkenes as well as cyclopentene and allene are summarized in Table 1. There exists site selectivity for unsymmetrical alkenes because of different insertion fashions, and the orientation of the substituents would establish different stereo-centers. Here, we only considered the pathway that leads to the formation of experimentally observed products. The free energy profiles of different substituted alkenes (see Fig. S9–S11†) are similar with that of ethylene as shown in Fig. 1b, except for styrene, in which the quintet insertion product **INT2<sub>Q</sub>** becomes more stable. There are two dominant contributions to the thermodynamic driving force for the radical-type migratory insertion, *i.e.*, the homolytic bond dissociation energy of Co–C bond and exergonicity of the addition of the carbon-centered radical to alkenes. The insertion reaction for all studied alkenes are thermodynamically favorable (Table 1), consistent with previous results of alkene insertion into M–C bonds of other transition-metal complexes.<sup>4a</sup>

**Table 1** Activation free energies ( $\Delta G^\ddagger$ ) and free energy changes ( $\Delta G^\circ$ )<sup>a</sup> during the migratory insertion step of cobalt-catalyzed aminoquinoline-directed coupling of C(sp<sup>2</sup>)–H bonds with different alkenes

Entry	Alkenes	Ref.	$\Delta G^\ddagger$	$\Delta G^\circ$
1		12a	12.3	–12.5
2		13a	14.5	–10.5
3		12a	16.3	–14.8
4		12a	16.9	–13.7
5		15b	16.2	–11.3
6		12a	17.3	–9.0
7		12a	16.1	–5.9
8		15a	18.8	–26.6

<sup>a</sup> The definition of  $\Delta G^\ddagger$  and  $\Delta G^\circ$  is given in Fig. 1b. All energies are in kcal mol<sup>–1</sup>.





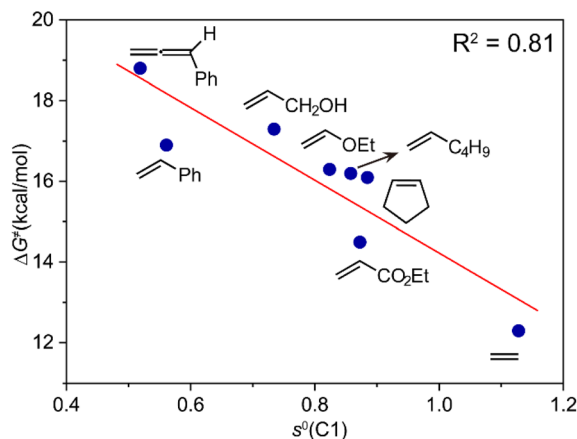


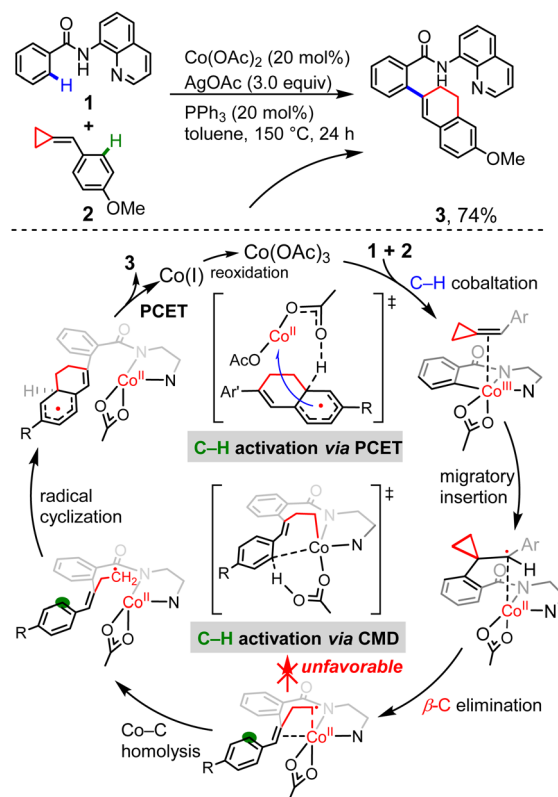
Fig. 3 Correlation of the activation free energy of the migratory insertion of different types of alkenes ( $\Delta G^\ddagger$ ) with the condensed local softness  $s^0$  of C1 atom that coordinates with cobalt in the transition state.

For the activation barriers of the migratory insertion of different alkenes into the same M–C bond, the values are mainly determined by the reactivity of radical addition. To rationalize the steric and electronic effects of the substituents on the activation barriers and to develop a predictable model for the reactivity of different types of coupling partners, we calculated the condensed local softness  $s^0$ , the values of which can be viewed as quantitative measures of the chemical reactivity of the different atoms in the molecule and are suited for studies of radical attack.<sup>23</sup> A relatively good correlation between the activation free energy of the migratory insertion and the condensed local softness of the C1 atom that coordinates to cobalt is observed (Fig. 3). The results again demonstrate the inherent radical character of the migratory insertion proposed. Other possible factors influencing the activation barriers are discussed in the ESI (Fig. S12–S14).<sup>†</sup> Apart from cobalt, the radical-type migratory insertion might also compete with classical insertion for other first-row transition metals that have smaller M–C bond dissociation energies in specific complexes.<sup>24</sup>

### The transition-metal-mediated ring opening strategy

Having established the radical-type insertion mechanism, we were particularly interested in its potential application to organic synthesis. The C–C activation catalyzed by transition metal complexes is a field of major interest, since it offers an efficient approach for the construction of organic compounds.<sup>25</sup> The highly strained, yet readily accessible alkylidenecyclopropanes can undergo a variety of ring-opening reactions and different modes of activation were observed.<sup>26</sup> Considering the diradical character of the insertion products generated in the aforementioned radical-type mechanism, we questioned whether the presence of cyclopropyl ring could enable new modes of C–C bond cleavage.

Despite the vast development of transition-metal-catalyzed ring-opening reactions and cycloadditions of ACPs, there are still limited reactions merging C–H activation and C–C bond



Scheme 2 The Co-catalyzed coupling reaction between benzamides and ACPs, and the originally proposed CMD mechanism together with the unconventional PCET mechanism proposed in this work.

cleavage.<sup>27–29</sup> Kwong and co-workers recently reported cobalt-catalyzed coupling between benzamides and ACPs *via* one-pot sequential activation of C–H/C–C/C–H bonds, generating the dihydronaphthalene skeletons (Scheme 2).<sup>10</sup> Based on a series of experimental mechanistic studies, Kwong proposed a plausible mechanism that involves N–H deprotonation, first C(sp<sup>2</sup>)–H activation, alkene insertion, β–C elimination, second C(sp<sup>2</sup>)–H activation *via* concerted metalation–deprotonation (CMD),<sup>30</sup> C–C reductive elimination and catalyst regeneration. Interestingly, our calculations show that, instead of the originally proposed CMD-type C–H activation, an unconventional proton-coupled electron transfer (PCET) is found to be the most favorable one. The cyclometallic intermediate formed by β–C elimination proceeds *via* unexpected Co–C homolysis to afford a cobalt(II) complex, which undergoes consecutive radical cyclization and PCET to afford the final product. In this proposed mechanism, we disclosed a new pattern of transition metal-mediated ring-opening process, which is the key step controlling the reaction selectivity.

The calculated reaction profiles for the cobalt-catalyzed chelation-assisted tandem C–H activation/C–C cleavage/C–H cyclization of aromatic amides with ACPs are depicted in Fig. 4. The possible roles of PPh<sub>3</sub> were not considered, since the product yield was indeed only slightly increased in the presence of ligand.<sup>10</sup> The three possible spin states of cobalt(III) were again investigated. Our calculations show that the reaction

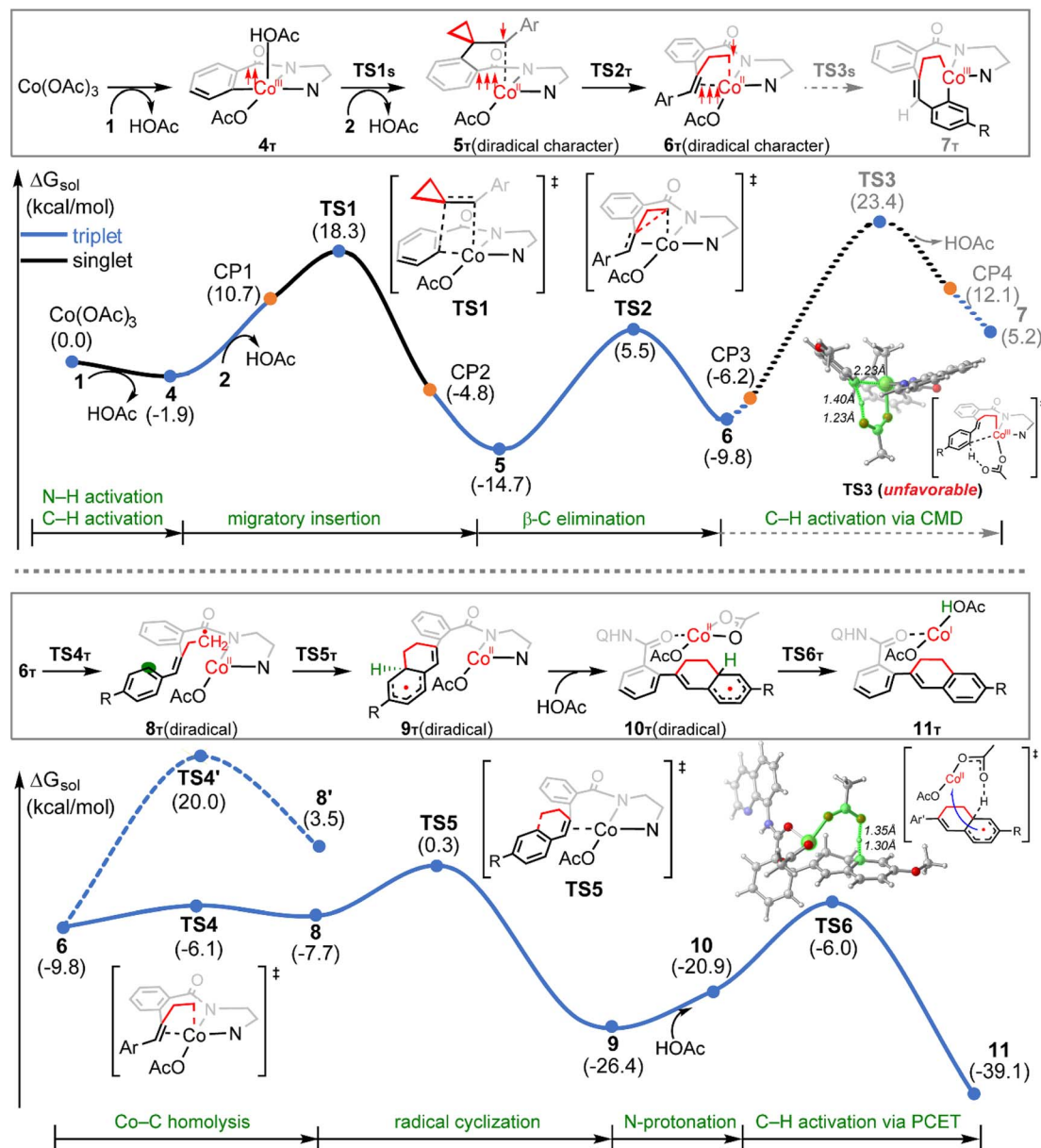


Fig. 4 Free energy profiles for the Co(III)-catalyzed tandem C–H activation/C–C cleavage/C–H cyclization process of aromatic amides with ACPs at the SMD(toluene)/B3LYP-D3(BJ)/def2-TZVP//SMD(toluene)/B3LYP-D3(BJ)/6-31G(d,p)/SDD(Co) level of theory. The skeletons of *N,N*-bidentate directing groups were simplified for clarity.

mainly proceeds on the singlet- and triplet-state surfaces, whereas the quintet-state is solely involved in the first N–H deprotonation. Previously, both experimental and computational studies demonstrated that an additional aminoquinoline-benzamide can coordinate with the metal center as a bis-chelating ligand.<sup>15b,31</sup> However, our calculations reveal that the migratory insertion of the ACP cannot take place from such bis-ligated intermediate, due to the significant steric repulsion between ACP and the additional amide unit (Fig. S15–S17†). The regioselectivity during the migratory insertion and the competition between C–N reductive elimination and ring opening *via*  $\beta$ -C elimination of the seven-membered cobaltacycle intermediate were also considered. The additional results are given in Fig. S18–S33.†

Initially, coordination of the amide nitrogen atom of the **1** to the active catalyst Co(OAc)<sub>3</sub> generates the substrate-coordinated intermediate. Then, facile N–H deprotonation and the first C(sp<sup>2</sup>)–H activation *via* base-assisted intramolecular electrophilic-type substitution (BIES)<sup>32</sup> take place to yield intermediate **4**, with the triplet state (4<sub>r</sub>) as the ground state. The effective activation barrier for the first C(sp<sup>2</sup>)–H activation is calculated to be 17.0 kcal mol<sup>−1</sup> (Fig. S15†). From complex 4<sub>r</sub>, the substrate–ligand exchange with **2** and the following radical-type insertion of alkene insertion into the newly formed Co–C bond lead to the formation of cobalt(II) intermediate **5<sub>r</sub>**, in which significant diradical character was observed (Fig. 5). Analogous to the results of alkenes shown in Fig. 1 and Table 1, a spin surface crossing through a minimum energy crossing

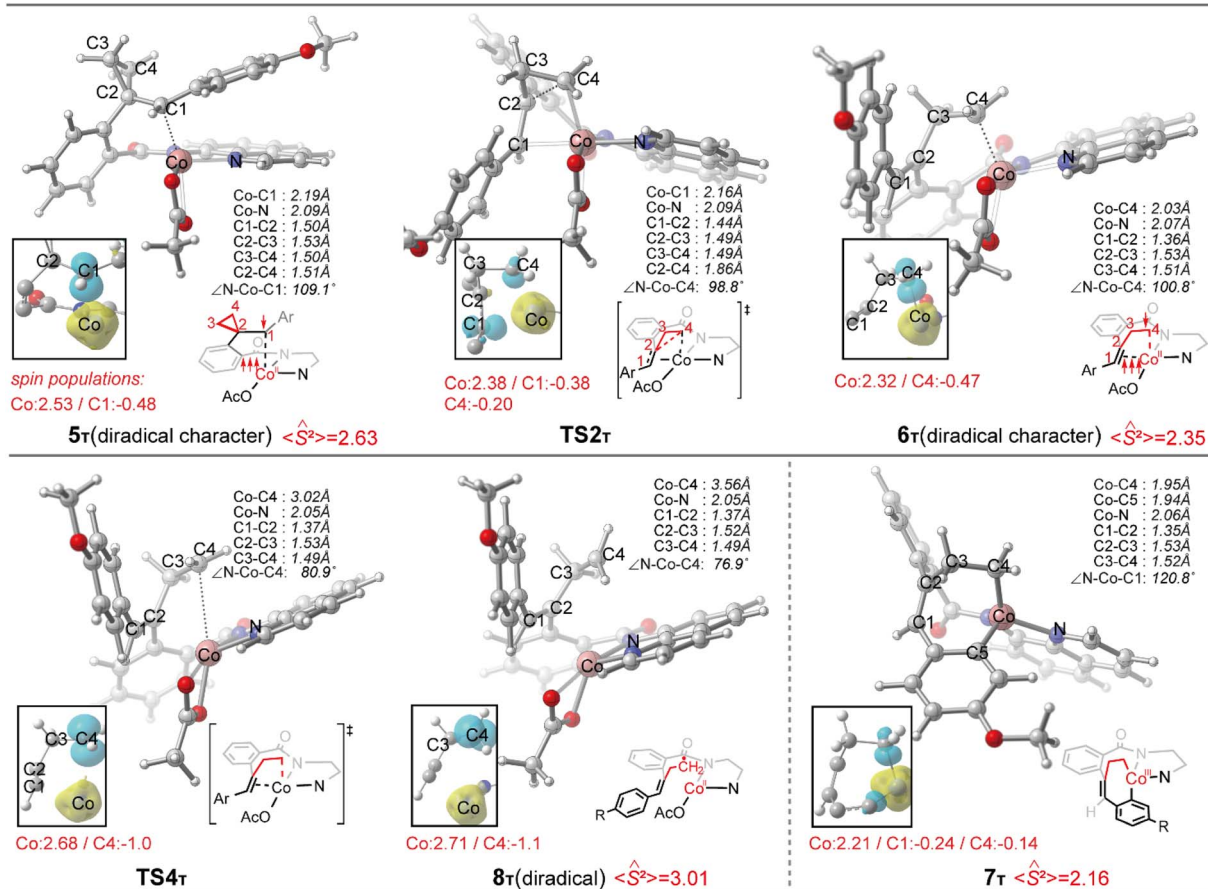


Fig. 5 Optimized structures of the key intermediates and transition states with truncated spin density contours (isovalue = 0.01, yellow:  $\alpha$ -spin density, cyan:  $\beta$ -spin density). The calculated spin populations and  $\langle \hat{S}^2 \rangle$  values are also given.

point (MECP; CP1 or CP2 in current case) between the triplet and singlet takes place prior to or after the migratory insertion transition state **TS1 $\tau$**  (Fig. 4). Subsequently, the  $\beta$ -C elimination takes place *via* **TS2 $\tau$** , wherein cleavage of a  $\beta$ -C-C  $\sigma$ -bond and formation of axial Co-C bond occur with concomitant generation of a  $\pi$ -bond. The corresponding optimized structures are depicted in Fig. 5. Upon formation of the eight-membered intermediate **6 $\tau$** , the second C(sp<sup>2</sup>)-H activation was originally proposed to proceed *via* the CMD-type transition state **TS3 $\tau$** , in which the coordinated acetate anion acts as the base for deprotonation *via* an inner-sphere mechanism. However, on the basis of our computational results, this process is kinetically unfavorable due to the relatively high energy barrier (**TS3 $\tau$** ,  $\Delta G^\ddagger = 38.1$  kcal mol<sup>-1</sup> relative to **5 $\tau$**  in Fig. 4). The feasibility of CMD mechanism can be further ruled out by considering that the transition state of the competing C-N reductive elimination from **6 $\tau$**  even lies below **TS3 $\tau$** , by 10.0 kcal mol<sup>-1</sup> (see Fig. S29†). Hong and co-workers recently found that the cobalt(IV) intermediate could be involved in both electro-chemical and chemical oxidation processes.<sup>33</sup> To address this possibility, a cobalt(IV) intermediate potentially generated from the oxidation of complex **6** by AgOAc was considered during the second C(sp<sup>2</sup>)-H activation. However, the Co(IV)-catalyzed C(sp<sup>2</sup>)-H activation is highly disfavored due to the significantly higher

barrier ( $\Delta G^\ddagger = 45.4$  kcal mol<sup>-1</sup> for the quartet states, see Fig. S27†). In addition, we also considered the possible roles of silver acetate,<sup>34</sup> but attempts to locate the corresponding transition states of bimetallic activation modes did not meet with success.

The pseudo-octahedral geometry of intermediate **6** and the existing ring strain prompted us to investigate the possible reaction pathway involving axial Co-C homolysis, analogous to the behavior observed in coenzyme B12.<sup>5</sup> Interestingly, as shown in Fig. 4, Co-C homolysis from **6 $\tau$**  is very facile, with a fairly low energy barrier. The resulting intermediate **8 $\tau$**  is a diradical, in which one of the unpaired electrons is located at the alkyl position (C4 atom, see Fig. 5) and the other three unpaired electrons are on the cobalt(II) center. The participation of this kind of complex is strongly supported by the radical quenching experiments, in which the yield of the product was significantly decreased, when 2,2,6,6-tetramethyl-1-piperidinyloxy (TEMPO) was added to the reaction medium and a compound generated by the radical-radical cross coupling reaction between intermediate **8 $\tau$**  and TEMPO was isolated.<sup>10</sup> Our calculations also revealed that the diradical **8 $\tau$**  cannot be directly formed *via* a single-step C-C cleavage from intermediate **5 $\tau$** .

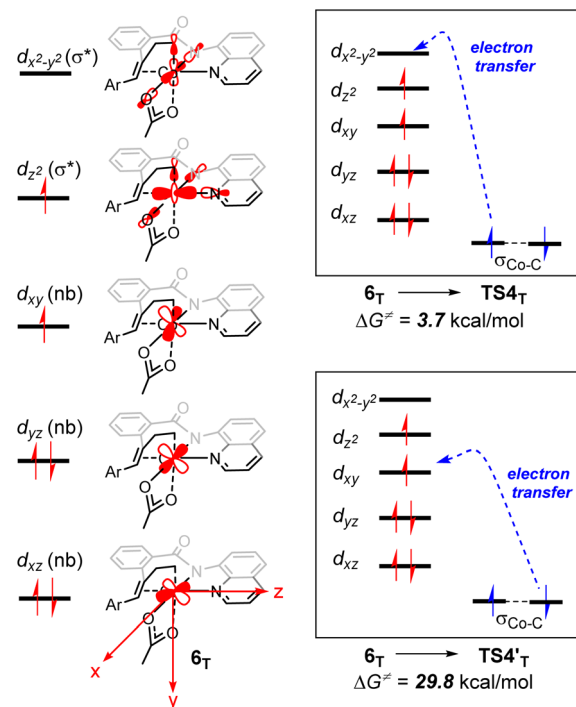




Instead, the abovementioned stepwise process involving  $\beta$ -C elimination ( $5_T \rightarrow 6_T$ ) and the subsequent Co–C homolysis ( $6_T \rightarrow 8_T$ ) is required. To achieve a deeper understanding of the cobalt-catalyzed radical-mediated carbon–carbon scission, the spin density distribution and the expectation value of the total spin ( $\langle \hat{S}^2 \rangle$ ) are used to assess the extent of the diradical character during this stepwise process (Fig. 5). As compared to  $8_T$ , intermediate  $5_T$  exhibit significant diradical character based on the relatively large spin densities distribution and the  $\langle \hat{S}^2 \rangle$  values. Furthermore, the diradical character decreases from intermediate  $5_T$  to  $6_T$  and then increases from  $6_T$  to  $8_T$ . In the diradical  $8_T$ , the distance between the cobalt(II) and the C4 atom is significantly long (up to 3.56 Å) with the alkyl radical pointing towards the phenyl ring.

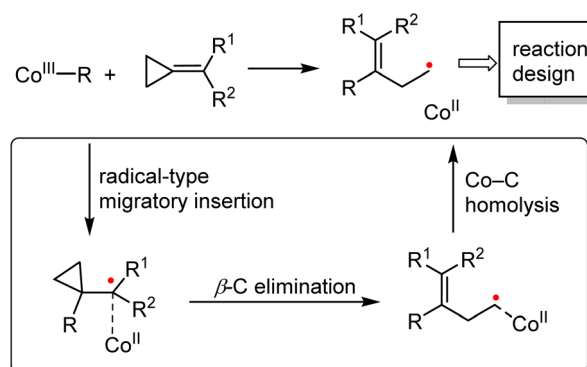
From  $8_T$ , an intramolecular cyclization by attack of the primary radical to phenyl ring *via* a favored six-membered transition state ( $TS5$ ) proceeds to afford the ring-closed intermediate  $9_T$ . Prior to the second C(sp<sup>2</sup>)–H activation, protonation is required for the cyclized intermediate  $9_T$ . The proton is transferred from an additional HOAc to the anionic N(sp<sup>3</sup>) atom of quinoline-based directing group, which only requires a barrier of 9.2 kcal mol<sup>−1</sup> (see Fig. S20†). The subsequent conformational changes make the O atom of 8-aminoquinoline rather than the N,N-bidentate directing group to become coordinated with cobalt(II) in  $10_T$ . The following C(sp<sup>2</sup>)–H activation requires 14.9 kcal mol<sup>−1</sup> from  $10_T$  to generate the product-coordinated complex  $11_T$ . Re-aromatization is realized *via* the PCET transition state  $TS6_T$ , which involves proton transfer from the sp<sup>3</sup> carbon to acetate and electron transfer from the cyclohexadienyl radical to the metal center. Compared to the results of the CMD mechanism (33.2 kcal mol<sup>−1</sup> for  $6_T$  to  $TS3_s$ ), the C(sp<sup>2</sup>)–H activation *via* PCET (20.4 kcal mol<sup>−1</sup> for  $9_T$  to  $TS6_T$ ) is significantly more favorable. Furthermore, the activation barrier of C(sp<sup>2</sup>)–H activation *via* PCET is 5.3 kcal mol<sup>−1</sup> lower than that of the competing C–N reductive elimination that produces spirocyclopropanes (Fig. S31†). This result successfully explains why the corresponding annulated product with conservation of the cyclopropyl ring was not observed in the experiments.<sup>10</sup> Finally, the cobalt(I) species dissociating from  $11_T$  is reoxidized into cobalt(III) to complete the catalytic cycle.

From  $6_T$ , we have located two different pathways for the homolytic cleavage of the Co–C bond, while the alternative Co–C homolysis *via*  $TS4_T$  (Fig. 4) is 26.1 kcal mol<sup>−1</sup> less favorable than that *via*  $TS4_T$ . The formation of radical intermediate  $8_T$  is also less thermodynamically favorable. The differences of the underlying electronic structure changes for the Co–C homolysis *via* the two pathways are illustrated in Scheme 3. For cobalt(II) complex  $6_T$ , the electronic structure can be described as  $(d_{xz})^2(d_{yz})^2(d_{xy})^1(d_{z^2})^1(d_{x^2-y^2})^0$ . For the homolysis *via* transition state  $TS4_T$ , an electron transfer from  $\sigma_{Co-C}$  orbital to the unoccupied  $d_{x^2-y^2}$ -based molecular orbital is calculated to be more favorable. The electron transfer to the antibonding orbital weakens the Co–C bond and lowers the corresponding reaction barrier. In the case of  $TS4_T$ , the electron transfer to the half-filled  $d_{xy}$  orbital results in considerable Coulomb repulsions, thus making this pathway unfavorable.



Scheme 3 Schematic molecular orbital diagrams with the electronic structure changes for the Co–C homolysis *via* two different pathways.

The organocobalt(III) complexes (Co<sup>III</sup>–R) and their radical activation reactions have been investigated for more than half a century. Cleavage of the Co–C bond *via* photolysis, electrochemistry, or thermolysis, producing the radicals in a controlled manner, is the fundamental step during such transformations.<sup>6b</sup> The strategy proposed herein (Scheme 4) clearly demonstrates that the strength of the Co–C bond is the key parameter that can lead to divergent reactivities as compared to the second- and third-row transition-metal complexes. Depending on the ligands and the alkyl group R, the single-electron pathway might be dominant for the cobalt complex. Furthermore, due to the persistent radical effect of Co(III)–R, which significantly extends the lifetime of the generated carbon-centered radicals, further selective inter- or



Scheme 4 Summary of the cobalt-catalyzed radical-mediated C–C bond cleavage/functionalization strategy.





intramolecular radical reactions could be developed on the basis of ring opening strategy.

## Conclusions

In summary, we have uncovered a radical-type migratory insertion mediated by cobalt(III) complex. The unprecedented radical-type insertion proceeds *via* concerted but asynchronous Co(III)–C homolysis and radical attack, which results in an insertion intermediate exhibiting diradical character. Depending on the coordination geometry as well as the oxidation and spin states, the radical-type insertion might compete favorably with the classical mechanism for the other first-row transition metals.

In combination with the use of alkylidenecyclopropanes, a new and fundamentally distinct cobalt-mediated ring opening strategy was further proposed. The strategy for C–C bond cleavage involves the radical-type addition of organocobalt(III) complexes into alkylidenecyclopropanes,  $\beta$ -carbon elimination and Co–C homolysis. This single-electron pathway is different from the behavior previously observed for palladium, nickel or rhodium-catalyzed C–C cleavages, in which redox-neutral  $\beta$ -carbon elimination usually occurs. Our mechanistic studies reveal that this cobalt-catalyzed radical-mediated C–C bond cleavage plays a key role in controlling the selectivity of cobalt-catalyzed coupling between benzamides and ACPs. Interestingly, the resulting carbon-centered radical undergoes facial intramolecular cyclization, followed by C(sp<sup>2</sup>)–H activation *via* PCET. The Co(III)/Co(II)/Co(I) catalytic scenario is significantly favored as compared to the originally proposed Co(III)/Co(I) pathway.

Finally, our results suggest that the low BDE of the Co–C bonds as well as the persistent radical effect with cobalt complexes can lead to distinct mechanisms for cobalt-catalyzed reactions, providing opportunities for achieving new reactivities that are inaccessible with other transition metals. We hope that our mechanistic insights will serve as an inspiration for further development of catalytic radical-type transformations.

## Computational details

All the geometries of the intermediates and transition states were optimized by Gaussian 09<sup>35</sup> in the corresponding solvent at the B3LYP<sup>36</sup>-D3(BJ)<sup>37</sup>/6-31G(d,p)/ECP10MDF(Co) level of theory with the corresponding Stuttgart/Dresden (SDD) effective core potential (ECP) on cobalt. Frequency calculations were performed at the same theoretical level to verify the nature of the stationary points and to obtain the thermal Gibbs free energy corrections ( $\Delta G_{\text{corr}}$ ) at 423.15 K (for ACPs) or 298.15 K (for the other alkenes). The intrinsic reaction coordinate (IRC)<sup>38</sup> calculations have been performed to confirm whether the obtained transition state is connected with two local minimum structures for a target reaction. Single point calculations at B3LYP-D3(BJ)/def2-TZVP<sup>39</sup> were carried out in solvent to obtain more accurate electronic energies. The continuum solvation model SMD<sup>40</sup> was utilized to consider the bulk solvent effects. Toluene is used as the solvent for ACPs and 2,2,2-

trifluoroethanol (TFE) is used as the solvent for the other alkene coupling partners. The correction caused by the different standard states in the gas phase and in solution was added to the free energies of all species. Numerical integrations were performed with the ultrafine grid during the calculations. The 3D diagrams of molecules and the spin density isosurface maps were prepared by CYLview<sup>41</sup> and GaussView5.0 respectively. The condensed local softness, atomic charges and spin densities were calculated by Multiwfn 3.8.<sup>42</sup>

## Data availability

Additional computational results supporting this work's conclusions are available in the ESI.†

## Author contributions

J.-B. L. and L. A. conceived the study, analyzed the results, and wrote the paper. J.-B. L., X.-J. L. and D.-Z. C. carried out the calculations. J. C. A. O. provided helpful discussions. All authors discussed the results and edited the paper.

## Conflicts of interest

There are no conflicts to declare.

## Acknowledgements

Financial support from Natural Science Foundation of Shandong Province (ZR2019YQ11) is gratefully acknowledged. L. A. thanks the DFG (Gottfried-Wilhelm-Leibniz-Preis to L. A. and SPP2363) and the European Union (ERC Advanced Grant No. 101021358).

## Notes and references

- For selected reviews and examples, see: (a) K. J. Cavell, *Coord. Chem. Rev.*, 1996, **155**, 209–243; (b) S. A. Macgregor and G. W. Neave, *Organometallics*, 2003, **22**, 4547–4556; (c) P. Wucher, L. Caporaso, P. Roesle, F. Ragone, L. Cavallo, S. Mecking and I. Göttker-Schnetmann, *Proc. Natl. Acad. Sci. U. S. A.*, 2011, **108**, 8955–8959; (d) P. S. Hanley and J. F. Hartwig, *Angew. Chem., Int. Ed.*, 2013, **52**, 8510–8525; (e) G. Lu, C. Fang, T. Xu, G. Dong and P. Liu, *J. Am. Chem. Soc.*, 2015, **137**, 8274–8283; (f) G. Huang and P. Liu, *ACS Catal.*, 2016, **6**, 809–820; (g) C. P. Richers, S. Roediger, V. Laserna and J. F. Hartwig, *Chem. Sci.*, 2020, **11**, 10449–10456.
- (a) R. F. Heck, *Acc. Chem. Res.*, 1979, **12**, 146–151; (b) I. P. Beletskaya and A. V. Cheprakov, *Chem. Rev.*, 2000, **100**, 3009–3066; (c) C. Amatore and A. Jutand, *Acc. Chem. Res.*, 2000, **33**, 314–321.
- (a) R. H. Grubbs and G. W. Coates, *Acc. Chem. Res.*, 1996, **29**, 85–93; (b) S. Mecking, *Angew. Chem., Int. Ed.*, 2001, **40**, 534–540; (c) V. C. Gibson and S. K. Spitzmesser, *Chem. Rev.*, 2003, **103**, 283–316.



- 4 (a) S. Niu and M. B. Hall, *Chem. Rev.*, 2000, **100**, 353–406; (b) X. Zhu, Y. Zheng and J. Liu, *J. Phys. Chem. A*, 2021, **125**, 5031–5039.
- 5 For selected reviews, see: (a) K. Gruber, B. Puffer and B. Kräutler, *Chem. Soc. Rev.*, 2011, **40**, 4346–4363; (b) M. Giedyk, K. Goliszewska and D. Gryko, *Chem. Soc. Rev.*, 2015, **44**, 3391–3404.
- 6 For selected reviews, see: (a) S. W. M. Crossley, C. Obradors, R. M. Martinez and R. A. Shenoi, *Chem. Rev.*, 2016, **116**, 8912–9000; (b) J. Demarteau, A. Debuigne and C. Detrembleur, *Chem. Rev.*, 2019, **119**, 6906–6955; (c) K. P. S. Cheung, S. Sarkar and V. Gevorgyan, *Chem. Rev.*, 2022, **122**, 1543–1625.
- 7 S. H. Kyne, G. Lefèvre, C. Ollivier, M. Petit, V. Ramis Cladera and L. Fensterbank, *Chem. Soc. Rev.*, 2020, **49**, 8501–8542.
- 8 (a) M. Moselage, J. Li and L. Ackermann, *ACS Catal.*, 2016, **6**, 498–525; (b) P. Gandeepan, T. Müller, D. Zell, G. Cera, S. Warratz and L. Ackermann, *Chem. Rev.*, 2019, **119**, 2192–2452; (c) P. Gandeepan, L. H. Finger, T. H. Meyer and L. Ackermann, *Chem. Soc. Rev.*, 2020, **49**, 4254–4272.
- 9 (a) W. I. Dzik, X. Xu, X. P. Zhang, J. N. H. Reek and B. de Bruin, *J. Am. Chem. Soc.*, 2010, **132**, 10891–10902; (b) H. Lu, W. I. Dzik, X. Xu, L. Wojtas, B. de Bruin and X. P. Zhang, *J. Am. Chem. Soc.*, 2011, **133**, 8518–8521; (c) C. F. Harris, C. S. Kuehner, J. Bacsá and J. D. Soper, *Angew. Chem., Int. Ed.*, 2018, **57**, 1311–1315; (d) M. Ociepa and D. Gryko, in *Cobalt Catalysis in Organic Synthesis*, ed. M. Hapke and G. Hilt, Wiley-VCH, Weinheim, Germany, 2020, pp. 417–451; (e) X. Cheng, X. Liu, S. Wang, Y. Hu, B. Hu, A. Lei and J. Li, *Nat. Commun.*, 2021, **12**, 4366.
- 10 M. Li and F. Y. Kwong, *Angew. Chem., Int. Ed.*, 2018, **57**, 6512–6516.
- 11 L. Grigorjeva and O. Daugulis, *Angew. Chem., Int. Ed.*, 2014, **53**, 10209–10212.
- 12 (a) L. Grigorjeva and O. Daugulis, *Org. Lett.*, 2014, **16**, 4684–4687; (b) L. Grigorjeva and O. Daugulis, *Org. Lett.*, 2014, **16**, 4688–4690; (c) T. T. Nguyen, L. Grigorjeva and O. Daugulis, *ACS Catal.*, 2016, **6**, 551–554.
- 13 (a) W. Ma and L. Ackermann, *ACS Catal.*, 2015, **5**, 2822–2825; (b) R. Mei, H. Wang, S. Warratz, S. A. Macgregor and L. Ackermann, *Chem.-Eur. J.*, 2016, **22**, 6759–6763; (c) N. Sauermann, T. H. Meyer, C. Tian and L. Ackermann, *J. Am. Chem. Soc.*, 2017, **139**, 18452–18455; (d) C. Tian, L. Massignan, T. H. Meyer and L. Ackermann, *Angew. Chem., Int. Ed.*, 2018, **57**, 2383–2387; (e) R. Mei, N. Sauermann, J. C. A. Oliveira and L. Ackermann, *J. Am. Chem. Soc.*, 2018, **140**, 7913–7921; (f) U. Dhawa, C. Tian, W. Li and L. Ackermann, *ACS Catal.*, 2020, **10**, 6457–6462.
- 14 (a) D. Kalsi and B. Sundararaju, *Org. Lett.*, 2015, **17**, 6118–6121; (b) D. Kalsi, S. Dutta, N. Barsu, M. Rueping and B. Sundararaju, *ACS Catal.*, 2018, **8**, 8115–8120.
- 15 (a) N. Thrimurtulu, A. Dey, D. Maiti and C. M. R. Volla, *Angew. Chem., Int. Ed.*, 2016, **55**, 12361–12365; (b) S. Maity, R. Kancherla, U. Dhawa, E. Hoque, S. Pimparkar and D. Maiti, *ACS Catal.*, 2016, **6**, 5493–5499; (c) A. Dey, N. Thrimurtulu and C. M. R. Volla, *Org. Lett.*, 2019, **21**, 3871–3875.
- 16 Z. Zhang, Y. Han, B. Zhan, S. Wang and B. Shi, *Angew. Chem., Int. Ed.*, 2017, **56**, 13145–13149.
- 17 (a) L. Zhang, X. Hao, Z. Liu, X. Zheng, S. Zhang, J. Niu and M. Song, *Angew. Chem., Int. Ed.*, 2015, **54**, 10012–10015; (b) P. Gandeepan, P. Rajamalli and C. Cheng, *Angew. Chem., Int. Ed.*, 2016, **55**, 4308–4311; (c) P. Williamson, A. Galván and M. J. Gaunt, *Chem. Sci.*, 2017, **8**, 2588–2591; (d) S. Tang, D. Wang, Y. Liu, L. Zeng and A. Lei, *Nat. Commun.*, 2018, **9**, 798; (e) S. Kathiravan and I. A. Nicholls, *Org. Lett.*, 2019, **21**, 9806–9811; (f) Y. Ban, L. You, T. Wang, L. Wu and Q. Liu, *ACS Catal.*, 2021, **11**, 5054–5060; (g) H. Zhai, M. Liu, C. Wang, S. Qiu, J. Wei, H. Yang and Y. Wu, *J. Org. Chem.*, 2021, **86**, 14915–14927.
- 18 (a) D. Schröder, S. Shaik and H. Schwarz, *Acc. Chem. Res.*, 2000, **33**, 139–145; (b) Y. Sun, H. Tang, K. Chen, L. Hu, J. Yao, S. Shaik and H. Chen, *J. Am. Chem. Soc.*, 2016, **138**, 3715–3730.
- 19 E. Ruiz, J. Cirera and S. Alvarez, *Coord. Chem. Rev.*, 2005, **249**, 2649–2660.
- 20 For selected examples, see: (a) D. A. Singleton, B. E. Schulmeier, C. Hang, A. A. Thomas, S. W. Leung and S. R. Merrigan, *Tetrahedron*, 2001, **57**, 5149–5160; (b) O. M. Gonzalez-James, E. E. Kwan and D. A. Singleton, *J. Am. Chem. Soc.*, 2012, **134**, 1914–1917; (c) Y. J. Hong, R. Ponc and D. J. Tantillo, *J. Phys. Chem. A*, 2012, **116**, 8902–8909; (d) S. R. Neufeldt, G. Jiménez-Osés, J. R. Huckins, O. R. Thiel and K. N. Houk, *J. Am. Chem. Soc.*, 2015, **137**, 9843–9854.
- 21 (a) P. V. R. Schleyer, C. Maerker, A. Dransfeld, H. Jiao and N. J. R. van Eikema Hommes, *J. Am. Chem. Soc.*, 1996, **118**, 6317–6318; (b) Z. Chen, C. S. Wannere, C. Corminboeuf, R. Puchta and P. V. R. Schleyer, *Chem. Rev.*, 2005, **105**, 3842–3888.
- 22 (a) N. Kumar, M. Alfonso-Prieto, C. Rovira, P. Lodowski, M. Jaworska and P. M. Kozłowski, *J. Chem. Theory Comput.*, 2011, **7**, 1541–1551; (b) G. M. Lee, A. S. C. Leung, D. J. Harrison, I. Korobkov, R. P. Hughes and R. T. Baker, *Organometallics*, 2017, **36**, 2853–2860; (c) P. Ma and H. Chen, *ACS Catal.*, 2019, **9**, 1962–1972; (d) N. P. van Leest and B. de Bruin, *Inorg. Chem.*, 2021, **60**, 8380–8387.
- 23 W. Yang and R. G. Parr, *Proc. Natl. Acad. Sci. U. S. A.*, 1985, **82**, 6723–6726.
- 24 (a) B. de Bruin, W. I. Dzik, S. Li and B. B. Wayland, *Chem.-Eur. J.*, 2009, **15**, 4312–4320; (b) O. Gutierrez, J. C. Tellis, D. N. Primer, G. A. Molander and M. C. Kozłowski, *J. Am. Chem. Soc.*, 2015, **137**, 4896–4899; (c) M. Yuan, Z. Song, S. O. Badir, G. A. Molander and O. Gutierrez, *J. Am. Chem. Soc.*, 2020, **142**(15), 7225–7234.
- 25 (a) C. Jun, *Chem. Soc. Rev.*, 2004, **33**, 610–618; (b) F. Chen, T. Wang and N. Jiao, *Chem. Rev.*, 2014, **114**, 8613–8661; (c) L. Souillart and N. Cramer, *Chem. Rev.*, 2015, **115**, 9410–9464; (d) P. Chen, B. A. Billett, T. Tsukamoto and G. Dong, *ACS Catal.*, 2017, **7**, 1340–1360; (e) L. Deng and G. Dong, *Trends Chem.*, 2020, **2**, 183–198; (f) M. Murakami and N. Ishida, *Chem. Rev.*, 2021, **121**, 264–299.
- 26 (a) A. Masarwa, D. Didier, T. Zabrodski, M. Schinkel, L. Ackermann and I. Marek, *Nature*, 2014, **505**, 199–203; (b)



- A. Brandi, S. Cicchi, F. M. Cordero and A. Goti, *Chem. Rev.*, 2014, **114**, 7317–7420; (c) D. S. Müller and I. Marek, *Chem. Soc. Rev.*, 2016, **45**, 4552–4566; (d) G. Fumagalli, S. Stanton and J. F. Bower, *Chem. Rev.*, 2017, **117**, 9404–9432; (e) Y. Cohen, A. Cohen and I. Marek, *Chem. Rev.*, 2021, **121**, 140–161.
- 27 (a) S. I. Kozhushkov, D. S. Yufit and L. Ackermann, *Org. Lett.*, 2008, **10**, 3409–3412; (b) L. Ackermann, S. I. Kozhushkov and D. S. Yufit, *Chem.–Eur. J.*, 2012, **18**, 12068–12077.
- 28 S. Cui, Y. Zhang and Q. Wu, *Chem. Sci.*, 2013, **4**, 3421–3426.
- 29 Y. Liang, V. Müller, W. Liu, A. Münch, D. Stalke and L. Ackermann, *Angew. Chem., Int. Ed.*, 2017, **56**, 9415–9419.
- 30 (a) D. Lapointe and K. Fagnou, *Chem. Lett.*, 2010, **39**, 1118–1126; (b) D. Balcells, E. Clot and O. Eisenstein, *Chem. Rev.*, 2010, **110**, 749–823; (c) L. Ackermann, *Chem. Rev.*, 2011, **111**, 1315–1345; (d) D. L. Davies, S. A. Macgregor and C. L. McMullin, *Chem. Rev.*, 2017, **117**, 8649–8709.
- 31 L. Xu, E. E. L. N. Liu, J. Bacsá, C. E. MacBeth and D. G. Musaev, *Chem. Sci.*, 2020, **11**, 6085–6096.
- 32 (a) W. Ma, R. Mei, G. Tenti and L. Ackermann, *Chem.–Eur. J.*, 2014, **20**, 15248–15251; (b) D. Zell, M. Bursch, V. Müller, S. Grimme and L. Ackermann, *Angew. Chem., Int. Ed.*, 2017, **56**, 10378–10382; (c) E. Tan, O. Quinonero, M. E. Orbe and A. M. Echavarren, *ACS Catal.*, 2018, **8**, 2166–2172; (d) L. Wang and B. P. Carrow, *ACS Catal.*, 2019, **9**, 6821–6836; (e) C. Zhu, R. Kuniyil, B. B. Jei and L. Ackermann, *ACS Catal.*, 2020, **10**, 4444–4450. See also Fig. S19† for details.
- 33 X. Chen, S. Zhang, T. H. Meyer, C. Yang, Q. Zhang, J. Liu, H. Xu, F. Cao, L. Ackermann and X. Hong, *Chem. Sci.*, 2020, **11**, 5790–5796.
- 34 (a) M. D. Lotz, N. M. Camasso, A. J. Canty and M. S. Sanford, *Organometallics*, 2017, **36**, 165–171; (b) B. Bhaskararao, S. Singh, M. Anand, P. Verma, P. Prakash, A. C. S. Malakar, H. F. Schaefer and R. B. Sunoj, *Chem. Sci.*, 2020, **11**, 208–216.
- 35 M. J. Frisch, G. W. Trucks, H. B. Schlegel, G. E. Scuseria, M. A. Robb, J. R. Cheeseman, G. Scalmani, V. Barone, B. Mennucci, G. A. Petersson, H. Nakatsuji, M. Caricato, X. Li, H. P. Hratchian, A. F. Izmaylov, J. Bloino, G. Zheng, J. L. Sonnenberg, M. Hada, M. Ehara, K. Toyota, R. Fukuda, J. Hasegawa, M. Ishida, T. Nakajima, Y. Honda, O. Kitao, H. Nakai, T. Vreven, J. A. Montgomery Jr, J. E. Peralta, F. Ogliaro, M. Bearpark, J. J. Heyd, E. Brothers, K. N. Kudin, V. N. Staroverov, R. Kobayashi, J. Normand, K. Raghavachari, A. Rendell, J. C. Burant, S. S. Iyengar, J. Tomasi, M. Cossi, N. Rega, J. M. Millam, M. Klene, J. E. Knox, J. B. Cross, V. Bakken, C. Adamo, J. Jaramillo, R. Gomperts, R. E. Stratmann, O. Yazyev, A. J. Austin, R. Cammi, C. Pomelli, J. W. Ochterski, R. L. Martin, K. Morokuma, V. G. Zakrzewski, G. A. Voth, P. Salvador, J. J. Dannenberg, S. Dapprich, A. D. Daniels, Ö. Farkas, J. B. Foresman, J. V. Ortiz, J. Cioslowski and D. J. Fox, *Gaussian 09 (Revision D.01)*, Gaussian, Inc., Wallingford CT, 2009.
- 36 (a) C. Lee, W. Yang and R. G. Parr, *Phys. Rev. B: Condens. Matter Mater. Phys.*, 1988, **37**, 785–789; (b) A. D. Becke, *J. Chem. Phys.*, 1993, **98**, 5648–5652.
- 37 S. Grimme, J. Antony, S. Ehrlich and H. Krieg, *J. Chem. Phys.*, 2010, **132**, 154104.
- 38 (a) K. Fukui, *Acc. Chem. Res.*, 1981, **14**, 363–368; (b) H. P. Hratchian and H. B. Schlegel, *J. Chem. Phys.*, 2004, **120**, 9918–9924.
- 39 (a) F. Weigend and R. Ahlrichs, *Phys. Chem. Chem. Phys.*, 2005, **7**, 3297–3305; (b) F. Weigend, *Phys. Chem. Chem. Phys.*, 2006, **8**, 1057–1065.
- 40 A. V. Marenich, C. J. Cramer and D. G. Truhlar, *J. Phys. Chem. B*, 2009, **113**, 6378–6396.
- 41 C. Y. Legault, *CYLview, 1.0b*, Université de Sherbrooke, Canada, 2009, <https://www.cylview.org>.
- 42 T. Lu and F. Chen, *J. Comput. Chem.*, 2012, **33**, 580–592.

